ELSEVIER

Exchange and fractionation of Mg isotopes between epsomite and saturated MgSO$_4$ solution

Weiqiang Li[*], Brian L. Beard, Clark M. Johnson

University of Wisconsin-Madison, Department of Geoscience, 1215 West Dayton Street, Madison, WI 53706, United States
NASA Astrobiology Institute, United States

Abstract

The equilibrium Mg isotope fractionation factor between epsomite and aqueous MgSO$_4$ solution has been measured using the three isotope method in recrystallization experiments conducted at 7, 20, and 40 °C. Complete or near-complete isotopic exchange was achieved within 14 days in all experiments. The Mg isotope exchange rate between epsomite and MgSO$_4$ solution is dependent on the temperature, epsomite seed crystal grain size, and experimental agitation method. The Mg isotope fractionation factors ($\Delta^{26}Mg_{eps-sol}$) at 7, 20, and 40 °C are $0.63 \pm 0.07‰$, $0.58 \pm 0.16‰$, and $0.56 \pm 0.03‰$, respectively. These values are indistinguishable within error, indicating that the Mg isotope composition of epsomite is relatively insensitive to temperature. The magnitude of the isotope fractionation factor ($\Delta^{26}Mg_{eps-sol}$ = ca. 0.6‰ between 7 and 40 °C) indicates that significant Mg isotope variations can be produced in evaporite sequences, and Mg isotopes may therefore, constrain the degree of closed-system behavior, paleo-humidity, and hydrological history of evaporative environments.
© 2011 Elsevier Ltd. All rights reserved.

1. INTRODUCTION

Magnesium sulfates are highly soluble minerals, and some forms of Mg sulfate (epsomite: MgSO$_4$·7H$_2$O, hexahydrite: MgSO$_4$·6H$_2$O and kieserite: MgSO$_4$·H$_2$O) are widespread and occur in Phanerozoic evaporate sequences (e.g., Hardie, 1990). Magnesium sulfate is also present on the surface of Mars, where, for example, up to 36 wt.% sulfate has been found in some outcrops on the Martian surface, of which Mg sulfate is the most abundant (Clark et al., 2005). On the Martian surface, sulfates are a major water reservoir and thus it is inferred that at least at one point in time aqueous alteration occurred on parts of the Martian surface (e.g., Wang et al., 2008).

High-precision measurements of stable Mg isotopes indicate that this isotope system holds great promise to fingerprint various geological and biogeochemical processes (e.g., Galy et al., 2002; Chang et al., 2004; Young and Galy, 2004; Pearson et al., 2006; Tipper et al., 2006; Pogge von Strandmann, 2008; Hippler et al., 2009; Shen et al., 2009; Bolou-Bi et al., 2010; Higgins and Schrag, 2010; Li et al., 2010). The majority of stable Mg isotope studies to date have focused on natural samples, and relatively few experimental determinations of stable Mg isotope fractionation factors have been made (e.g., Kisakurek et al., 2009; Immenhauser et al., 2010). There have been no studies of the isotopic fractionation of Mg between sulfates and saturated solutions.

In this study, a recrystallization approach was used to determine the equilibrium Mg isotope fractionation factor between solid and aqueous phases of MgSO$_4$ at 7, 20, and 40 °C. A ^{25}Mg-enriched tracer was used to constrain the rate and extent of isotopic exchange between the two phases, following the "three-isotope exchange method" that has been applied to oxygen and iron isotope systems (e.g., Matsuhisa et al., 1978; Matthews et al., 1983a,b; Shahar et al., 2008; Beard et al., 2010). This study is the first to apply the "three-isotope exchange method" to the Mg isotope system at low temperature. Our results demonstrate

---

* Corresponding author. Tel.: +1 6087727386.
E-mail addresses: liweiq@gmail.com, wli@geology.wisc.edu (W. Li).

that the isotopic exchange between epsomite and solution is rapid and that heavier Mg isotopes preferentially partition into epsomite relative to the solution under equilibrium conditions.

2. ANALYTICAL METHODS

Magnesium isotope measurements were made using a Micromass *IsoProbe* MC-ICP-MS, a single-focusing mass spectrometer that uses a collision cell to thermalize the ion beam. Helium was used as the collision gas for thermalization and H$_2$ was used as a reactive gas to minimize isobaric interferences at masses 25 and 26, which are thought to be $^1H^{12}C_2$ and $^{12}C^{14}N$, respectively. Because these samples are enriched in ^{25}Mg, complete washout between samples that have large differences in Mg isotope composition by up to $\sim$20‰ in $^{25}Mg/^{24}Mg$ is critical, and thus we employ the methods developed by Beard et al. (2010) to minimize wash-out effects by using a wet plasma and reducing the cone voltage of the *IsoProbe*. Magnesium solutions were introduced into the Ar plasma using a self-aspirating 100 μL/min nebulizer tip and a cyclonic spray chamber cooled to 5 °C, and the cone voltage was set to 50–80 V. These conditions produce a total Mg ion intensity of 5×10^{-11} A using a 3 ppm Mg solution. Washout between samples used a 2% HNO$_3$ solution for 6 min. Overall, the "on-peak" blank acid produced a typical ion intensity of 1.2×10^{-17}, -1.7×10^{-16}, and -7.8×10^{-16} A at masses 25, 24, and 26, respectively that did not change during an analytical session.

Magnesium isotope ratios were determined using a sample-standard bracketing technique. Samples were typically diluted to 3 ppm $\pm$5%. Matrix effects associated with Mg concentration were corrected by analysis of the standard solution diluted over a range of 1.5–4.5 ppm Mg, following methods discussed by Albarède and Beard (2004), which typically resulted in a correction of less than 0.02‰ in $^{26}Mg/^{24}Mg$ for the samples. Isotope ratios are subtracted for on-peak zeros using a 30 s on-peak acid blank measurement prior to forty 10-s on-peak integrations of the analyte solution. This measurement routine results in a typical internal (2 standard error) precision of better than $\pm$0.04‰ in $^{26}Mg/^{24}Mg$ and $\pm$0.02‰ for $^{25}Mg/^{24}Mg$.

Prior to isotope analysis, saturated MgSO$_4$ solutions or epsomite samples were dissolved in 200 μL 0.2 M HCl and loaded onto an ion-exchange column that contained 0.3 mL of Biorad AG MP-50 cation exchange resin that had been pre-conditioned with 2 mL 0.2 M HCl. Sulfate was eluted using 3 mL 0.2 M HCl, and Mg^{2+} was quantitatively removed using 3 mL 6 M HCl. The MgCl$_2$ solution was heated at 120 °C with five drops of concentrated HNO$_3$ and three drops of 30% H$_2$O$_2$ to dryness three times to convert the Mg salt into the nitric form. Recovery of Mg was >90% and yields were determined spectrophotometrically using the calmagite colorimetric method (Chauhan and Ray Sarkar, 1969). We note that the slightly less than 100% recovery may be caused by bubbling during H$_2$O$_2$ treatment, and therefore does not reflect loss on the columns.

We evaluated this ion-exchange method for bias in Mg isotope data by analysis of an in-house Mg standard solution that was passed through the ion-exchange column procedure, and the measured isotopic composition of these samples match the isotopic composition of this standard (Table 1). Moreover, we evaluated matrix effects by spiking the ultrapure Mg standard solution with H$_2$SO$_4$ to produce a solution with a $\sim$1.5:1 M sulfate to Mg ratio, and this purified solution matches the Mg isotope composition of the unadulterated sample. Total Mg procedural blanks were determined using isotope dilution and a ^{26}Mg spike, and were 9.4 ± 3.7 ng (2 SD, $n = 2$), which is negligible (<0.01% of the Mg in a sample). Accuracy and external precision of Mg isotope ratio measurements were evaluated by analysis of four ultrapure Mg standard solutions that defined a $\sim$3‰ spread is $^{26}Mg/^{24}Mg$ (Table 1). The external long-term reproducibility (2 SD) of this technique is better than 0.15‰ for $^{26}Mg/^{24}Mg$ and 0.1‰ for $^{25}Mg/^{24}Mg$, as determined by replicate analyses of the four ultrapure Mg standard solutions. The accuracy of this method is shown by the reproducibility of the Mg isotope composition of two recognized Mg isotope standards, DSM3 and Cambridge1 (Galy et al., 2003; Table 1), as well as 10 analyses of in-house Mg standard that were processed through the entire analytical method that produced the same isotopic composition as the pure solution (Table 1).

Magnesium isotope compositions are reported using the standard per mil (‰) notation of $\delta^{26}Mg$ and $\delta^{25}Mg$ for the $^{26}Mg/^{24}Mg$ and $^{25}Mg/^{24}Mg$ isotope ratios, respectively, where

$$\delta^{26}Mg = [(^{26}Mg/^{24}Mg_{sample})/(^{26}Mg/^{24}Mg_{DSM3}) - 1] * 1000 \tag{1}$$

$$\delta^{25}Mg = [(^{25}Mg/^{24}Mg_{sample})/(^{25}Mg/^{24}Mg_{DSM3}) - 1] * 1000 \tag{2}$$

DSM3 is the international Mg isotope standard (Galy et al., 2003). Fractionation in Mg isotope compositions between two phases A and B is expressed as:

$$\Delta^{26}Mg_{A-B} = \delta^{26}Mg_A - \delta^{26}Mg_B \approx 10^3 \ln \alpha^{26/24}_{A-B} \tag{3}$$

$$\Delta^{25}Mg_{A-B} = \delta^{25}Mg_A - \delta^{25}Mg_B \approx 10^3 \ln \alpha^{25/24}_{A-B} \tag{4}$$

Note that the $\Delta^{25}Mg_{A-B}$ defined here is different from the $\Delta^{25}Mg'$ parameter, which has been used to discern the existence of radiogenic $^{26}Mg^*$ due to decay of the short-lived ^{26}Al in meteorites, or to evaluate subtle differences between equilibrium and kinetic mass-dependent fractionation laws (e.g., Young et al., 2002; Young and Galy, 2004).

3. EXPERIMENT DESIGN

We employed a "three-isotope" method (e.g., Matsuhisa et al., 1978; Matthews et al., 1983a,b; Shahar et al., 2008; Beard et al., 2010) to evaluate the Mg isotope exchange kinetics and approach to Mg isotope equilibrium between epsomite and saturated MgSO$_4$ solutions at 7, 20, and 40 °C. Magnesium isotope exchange was promoted by a recrystallization process, where fine-grained epsomite seed crystals were suspended in saturated MgSO$_4$ solutions and the epsomite crystals recrystallized into coarser grains. This recrystallization process is termed "Ostwald ripening",

Table 1
Mg isotope compositions and external precisions of standards and test solutions passed through ion-exchange chromatography. Analyses were made using HPS909104 as the in-house Mg isotope standard, and data are reported relative to DSM3.

Sample	$\delta^{26}Mg$	2SD	$\delta^{25}Mg$	2SD	n
Isotope standards					
DSM3	0.00	0.12	0.00	0.08	59
Cambridge1	−2.57	0.15	−1.32	0.09	48
NBS980	−4.13	0.08	−2.09	0.07	33
HPS909104	−0.67	0.10	−0.35	0.07	28
HPS932001	−2.93	0.14	−1.49	0.09	47
Isotope composition of Cambridge1 in reference (selected)					
Cambridge1 (Galy et al., 2003)	−2.58	0.14	−1.33	0.07	35
Cambridge1 (Tipper et al., 2006)	−2.60	0.14	−1.34	0.08	168
Cambridge1 (Pearson et al., 2006)	−2.57	0.13	−1.34	0.04	69
Cambridge1 (Hippler et al., 2009)	−2.58	0.04	−1.34	0.02	56
Cambridge1 (Huang et al., 2009)	−2.63	0.11	−1.36	0.07	44
Test solutions processed through ion-exchange columns					
50 µg HPS909104	−0.71	0.02	−0.38	0.03	3[a]
100 µg HPS909104	−0.65	0.09	−0.33	0.11	5[a]
100 µg HPS909104 + 6 µmol H_2SO_4	−0.64	0.11	−0.31	0.02	2

[a] Denotes the number of complete procedural replicates dispersed in analytical sessions with samples.

where the growth of larger crystals occurs through dissolution of smaller crystals (e.g., Stoffregen et al., 1994). It is important to note that the concentration of the $MgSO_4$ solution did not change with time in these experiments, indicating that there was no net mass transfer of Mg. This recrystallization experimental technique is an excellent method for promoting equilibrium isotope exchange because recrystallization experiments are less likely to incorporate kinetic effects relative to those that employ a simple synthesis approach, as the free-energy changes that drive recrystallization tend to be much smaller, on the order of those associated with isotopic exchange (Matthews et al., 1983a). Moreover, this recrystallization approach is the only effective way to attain isotopic exchange at low temperatures (<100 °C), because isotope exchange via solid-state diffusion is only practical at high temperatures.

The three-isotope method involves isotope exchange between two components, where one component contains "normal" Mg and the other component is enriched in ^{25}Mg. On a $\delta^{25}Mg$–$\delta^{26}Mg$ diagram, all terrestrial samples that have normal Mg isotope compositions plot on a line with a slope of about 0.52, which is defined as the primary or terrestrial fractionation line (for more details, see Young and Galy, 2004). The component that has natural Mg plots on the terrestrial fractionation line, but the component that is spiked with ^{25}Mg does not (Fig. 1). As the two components undergo isotopic exchange, their isotopic compositions evolve toward isotopic equilibrium. At isotopic equilibrium, the two components will lie along a secondary mass-fractionation line that is parallel to the terrestrial fractionation line, whose position on a $\delta^{25}Mg$–$\delta^{26}Mg$ plot is dictated by the isotopic mass balance of the two components (Fig. 1). In our experiments we used an enriched-^{25}Mg isotope tracer, where a ^{25}Mg-enriched $MgSO_4$ solution was reacted with epsomite that had "normal" isotope composition, as well as the reverse, where the $MgSO_4$ solution with "normal" isotope composition was reacted

that had ^{25}Mg-enriched epsomite. The enriched ^{25}Mg spike (^{24}Mg: 0.80%, ^{25}Mg: 98.88%, ^{26}Mg: 0.32%) was obtained from Oak Ridge National Lab. The spike and natural Mg were mixed with a ratio of about 1:500 for preparing the spiked starting material that had a $\delta^{25}Mg$ value of ca. 19‰. The amount of ^{26}Mg and ^{24}Mg from the spike is negligible compared to the bulk Mg and the $^{26}Mg/^{24}Mg$ ratio of the natural Mg is basically unchanged after spiking (<0.03‰ shift).

The recrystallization experiments were carried out at three different temperatures (7 °C: Experiments 7A, 7B; 20 °C: Experiments 20A, 20B; 40 °C: Experiments 40A, 40B. Fig. 2 and Table 2), using both the normal epsomite (A-series) and ^{25}Mg-enriched epsomite (B-series) for the starting crystals. All experimental reagents were thermally stabilized for 2 days before mixing. Experiments at 7 and 20 °C were carried out in a walk-in refrigerator and air-conditioned room, respectively. The temperature variation during the experiments at 7 and 20 °C was monitored with thermometers and estimated to be ±1 °C. Based on the solubility data for epsomite (Archer and Rard, 1998; Mullin, 2001), a 2 °C variation in temperature would cause the Mg concentration of the $MgSO_4$ solution to vary by 3.2% at 7 °C and 2.7% at 20 °C. These variations lie within the range of the direct measurement of Mg concentration of the $MgSO_4$ solution using isotope dilution (shown in the following section), indicating no significant net dissolution or precipitation, despite extensive recrystallization. Experiments at 40 °C were carried out in a water bath where temperature varied less than ±0.1 °C.

Each experiment used 10–20 centrifuge tubes of identically prepared mixtures of crystals and solution, where individual tubes were sacrificed and sampled for isotopic analysis for time-series sampling. Centrifuge tubes were sealed to minimize fluid loss during re-crystallization, and tests showed that the daily loss of H_2O was <0.05 mg at 7 °C, <0.2 mg at 20 °C, and <0.4 mg at 40 °C. Net
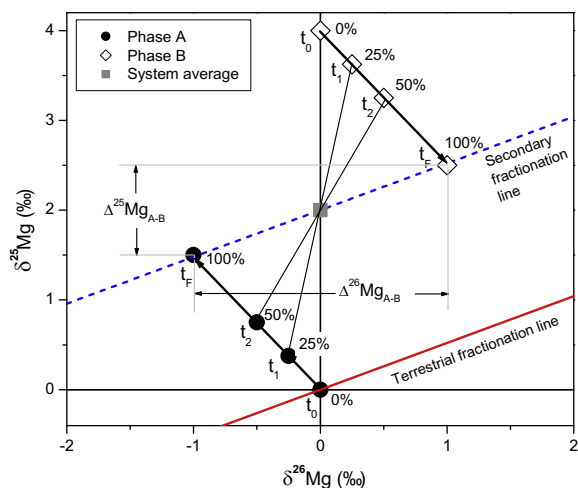
Fig. 1. Schematic diagram of the three-isotope method as applied to Mg. Phase A initially has a natural Mg isotope composition and plots on the terrestrial fractionation line. The slope of the terrestrial fractionation line follows a mass-dependent law (Young and Galy, 2004). As plotted, phase B initially has the same δ^{26}Mg value as phase A (this need not always be the case), but is offset from the terrestrial fractionation line due to the presence of a ^{25}Mg spike. As isotopic exchange between the two phases proceeds, the isotopic compositions of the two evolve toward a value that reflects 100% isotopic exchange. Note that at any time, a line connecting the two phases on the three-isotope plots crosses the system average because of isotope mass balance. When complete isotopic exchange is reached, the isotopic compositions of phases A and B will lie on a secondary fractionation line, which is parallel to the terrestrial fractionation line. Note that the position of the secondary fractionation line is controlled by the isotopic mass balance of the system. If the isotopic exchange is slow and incomplete, the isotopic compositions at 100% exchange (t_F) can be obtained by extrapolation of the time-series (t_0, t_1, t_2, ...) isotope data to the secondary fractionation line. If isotopic exchange occurs under equilibrium conditions, the extrapolated value at 100% exchange will be equal to the equilibrium isotope fractionation factor.

Fig. 2. Phase diagram of MgSO₄ hydrates, modified from Chou and Seal (2003) and Posern and Kaps (2008). The dark star denotes the temperature and humidity conditions during initial synthesis of fine-grained epsomite. The gray line is the humidity-buffer curve for air in equilibrium with saturated NaCl solution. The three gray circles denote the conditions of the isotope exchange experiments in this study.

precipitation of epsomite caused by leaking of water vapor are therefore, insignificant relative to the large weight of the starting MgSO₄ solution (>350 mg). Each centrifuge tube was loaded with 0.10–0.13 g of epsomite, and between 0.2 and 0.4 mL of saturated MgSO₄ solution; all weights and volumes were measured precisely to monitor mass balance. The variation in the molar ratio of Mg contained in epsomite and saturated MgSO₄ solution in different centrifuge tubes was <2%. Centrifuge tubes were constantly mixed on a roller or an orbital shaker, and Table 2 contains a summary of experimental conditions.

Centrifuge tubes were sampled in a time series in an exponential fashion (e.g., 1 day, 2 day, 4 day, 8 days ...), and most samples were duplicated at each time. Separation of the supernatant from the epsomite was initially carried out by centrifugation (5000 rpm for >5 min). Supernatant was then extracted and filtered using a 0.45 μm nylon syringe filter to ensure that the MgSO₄ solution was free of epsomite. Epsomite retained in the centrifuge tubes was washed twice with 0.7 mL 40% (vol/vol) ethanol solution, followed by shaking, centrifugation and removal of the
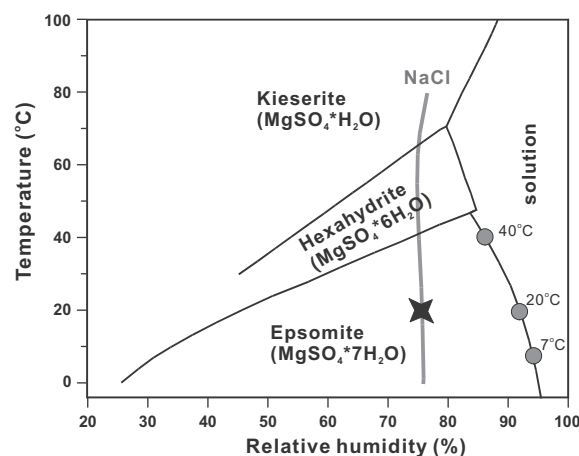
ethanol; washing with 40% ethanol is essential for removing the interstitial MgSO₄ solution with negligible dissolution of epsomite crystals. For experiments at 7 and 20 °C, these procedures were carried out in a walk-in refrigerator and air-conditioned room, respectively, at the same temperatures of the experiments. For experiments at 40 °C, separation was carried out in an oven with temperature set at 40 °C. In all cases, the centrifuge, all the syringes, filters and the ethanol solution were equilibrated at the experiment temperature for >5 h prior to separation. The washed epsomite was split into two aliquots; one aliquot was used for XRD analysis, which confirmed that all reacted solids were epsomite, and the other aliquot was dissolved in 0.2 mL of 0.2 M HCl and processed through ion-exchange columns for Mg isotope analysis.

Commercially available epsomite is too coarse-grained (0.1–1 mm diameter) to permit recrystallization on reasonable experimental time-scales, and reduction in size via grinding is not practical because crushing produces a phase transition from epsomite (MgSO₄·7H₂O) to hexahydrite (MgSO₄·6H₂O), as well as a heterogeneous size distribution (Electronic Appendix 1). We therefore, developed two methods to synthesize fine-grained epsomite of relatively uniform grain size. One method produced finer-grained epsomite than the other. In general, epsomite was synthesized by preparing a saturated MgSO₄ solution at 20 ± 1 °C, followed by initiation of precipitation by addition of 100% ethanol to the solution while the material was being sonicated in an ultrasonicator. Ethanol has a high affinity for H₂O, which induces oversaturation and epsomite precipitation; ultrasonic agitation suspended the newly-formed epsomite crystals into the bulk ethanol solution, which produced a fine-grained and homogeneous epsomite suspension of small crystals. The different epsomite grain sizes were produced by using different rates of ethanol addition to the saturated MgSO₄ solution and the manner in which

Table 2
Summary of experiments.

Experiment series ID	Temperature (°C)	Agitation method	Starting material	Initial average epsomite crystal size (μm)	Final average epsomite crystal size	Molar ratio of magnesium Mg_{sol}/Mg_{eps}
7A	7 ± 1	Roller	Isotopically normal epsomite + spiked MgSO$_4$ solution	2–5	150 × 700 μm @ 31 days	1.56 ± 0.04
7B	7 ± 1	Roller	Spiked epsomite + isotopically normal MgSO$_4$ solution	30–50	100 × 500 μm @ 15 days	1.56 ± 0.04
20A	20 ± 1	Roller	Isotopically normal epsomite + spiked MgSO$_4$ solution	2–5	300 × 800 μm @ 65 days	1.83 ± 0.04
20B	20 ± 1	Roller	Spiked epsomite + isotopically normal MgSO$_4$ solution	30–50	300 × 800 μm @ 64 days	1.85 ± 0.02
40A	40 ± 0.1	Orbital shaker	Isotopically normal epsomite + spiked MgSO$_4$ solution	2–5	300 × 1000 μm @ 16 days	2.35 ± 0.04
40B	40 ± 0.1	Orbital shaker	Spiked epsomite + isotopically normal MgSO$_4$ solution	30–50	200 × 800 μm @ 15 days	2.35 ± 0.04

the ethanol plus MgSO$_4$ solution was mixed via shaking and ultrasonication. Fine-grained epsomite was synthesized by adding 0.6 mL of saturated MgSO$_4$ solution to 30 mL of ethanol over 6 min in an ultrasonic bath, following by 40 min of ultrasonic treatment. This finer-grained epsomite was made using Mg that had a "normal" Mg isotope composition and the average grain size was 2–5 μm (see below). The coarser-grained epsomite was made using a ^{25}Mg-enriched solution. This epsomite was synthesized by adding 30 mL of ethanol to 3 mL of the saturated ^{25}Mg-enriched MgSO$_4$ solution and shaking, followed by ultrasonicating for 25 min. This technique produced epsomite that had an average grain size of 30–50 μm.

All synthesized epsomite was separated from the solution by transferring the mixture to 30 mL centrifuge tubes and centrifuging at 4500 rpm for 10 min. The solution was decanted, and the epsomite was dried by purging the headspace with N$_2$ gas flowing at 10 mL/min. In order to avoid phase transformation, the N$_2$ gas was initially bubbled through a saturated aqueous NaCl solution at 20 °C, which buffers the gas to a humidity of 76%, which is within the stability field of epsomite (Electronic Appendix 2; Fig. 2). Gas purging was done until the weight of the centrifuge tube was constant to within ±5 mg, which took approximately 7 days.

The synthesized materials before and after N$_2$ purging were confirmed to be pure epsomite by XRD analysis. We were not able to determine the surface area of the epsomite by BET because epsomite looses water and transforms to other phases rapidly under vacuum. We therefore, determined the approximate size of epsomite via SEM and optical microscopy (Electronic Appendix 3; Fig. 3), which showed that the finer-grained, isotopically "normal" epsomite varied between 0.5 and 10 μm in size of the elongated dimension (average 2–5 μm). The coarser-grained, ^{25}Mg-enriched epsomite varied between 5 and 100 μm in size of the elongated dimension (average 30–50 μm). No fluid inclusions were observed in the epsomite crystals.

4. RESULTS

The grain size of the epsomite increased significantly during the experiments (Fig. 3). Growth of epsomite was continuous throughout the experiment period, although the most dramatic change in grain size occurred at the beginning of the experiments. For example, in Experiment 20A (normal epsomite + spiked solution at 20 °C; Table 2), the grain size of epsomite increased from 2–5 μm to ca. 20 × 100 μm after 1 day, further grew up to 50 × 150 μm after 4 days, and after 65 days the average size of the epsomite grains were about 200 × 500 μm. The growth of epsomite in Experiment 20B is similar except that the grain size was relatively larger in the early stages of the recrystallization experiment (Fig. 3), which is likely due to the larger starting grain size. Recrystallization at 40 °C produced the most rapid increase in crystal size. At this temperature, the epsomite grains after 15 days of recrystallization were larger than the epsomite grains after 60 days of recrystallization at 20 °C (Table 2). Growth of epsomite at 7 °C was the slowest. The morphology of the recrystallized epsomite at 7 °C was also distinct, and had
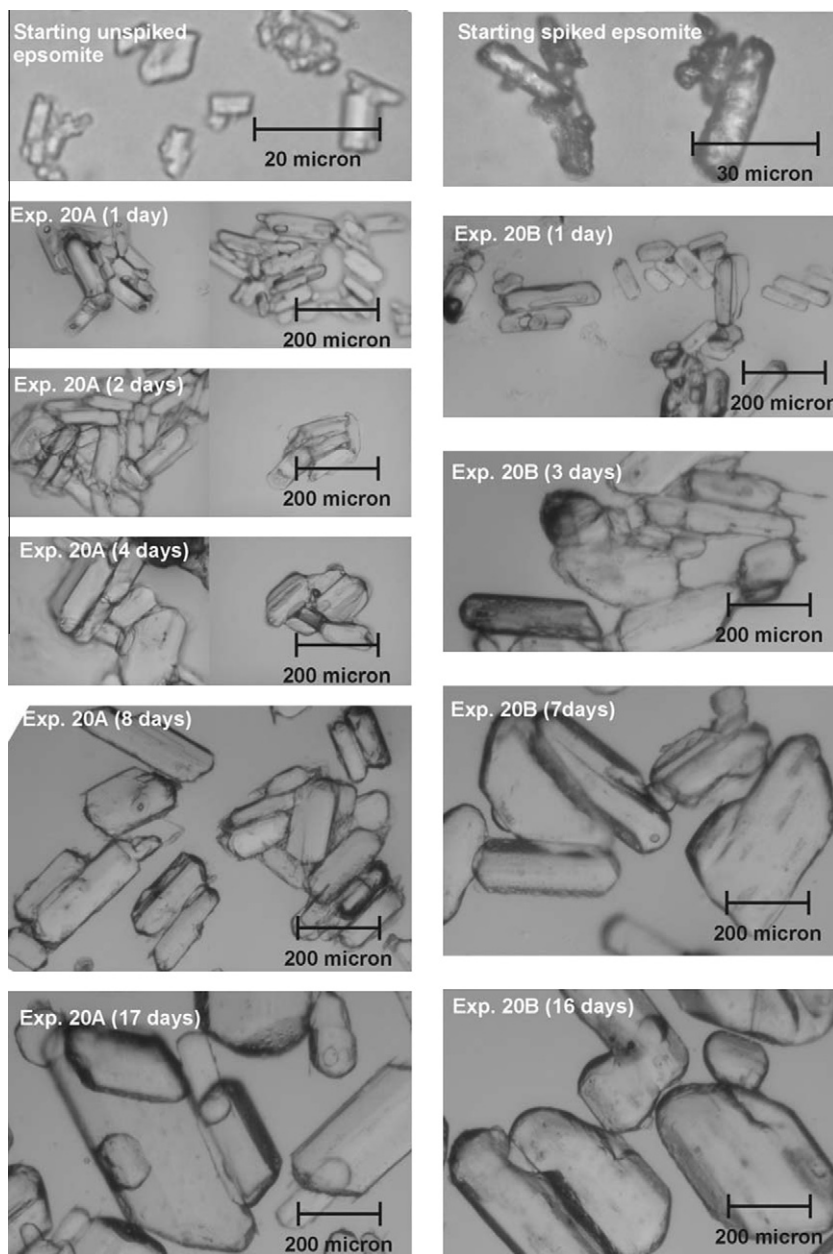
Fig. 3. Photomicrographs of representative epsomite grains at different time points for experiments run at 20 °C.

more elongated shapes than epsomite produced in the 20 and 40 °C experiments (Table 2).

The concentration of Mg in the solutions for all experiments remained constant within the uncertainty of the concentration estimates based on Mg ion intensity during isotopic analysis and by spectrophotometry. This uncertainty was likely ±10% to 20% when considering dilution errors associated with the highly concentrated MgSO₄ solutions. In order to more rigorously evaluate if there was net mass transfer during the re-crystallization experiments, a series of normal epsomite and normal saturated MgSO₄ solutions were prepared and allowed to recrystallize over the same time duration as the ^{25}Mg-enriched experiments and the concentration of the MgSO₄ solution was measured

using isotope dilution mass spectrometry. These high-precision concentration measurements show that the there was no variability in the Mg concentration, confirming that there was no net mass transfer in the recrystallization experiments (Fig. 4).

The Mg isotope compositions of epsomite and MgSO₄ solution in the recrystallization experiments varied with time, and the general temporal trends of δ^{26}Mg and δ^{25}Mg values for epsomite and MgSO₄ solutions were very similar (Figs. 5–7; Electronic Appendix 4). Generally speaking, the starting epsomite and MgSO₄ solution had similar δ^{26}Mg values (ca. −0.4 to −0.5‰) and these diverged within 1–7 days, and remained constant at δ^{26}Mg$_{eps}$ = −0.1 to −0.2‰ and δ^{26}Mg$_{sol}$ = −0.7 to −0.8‰ for the remainder of the
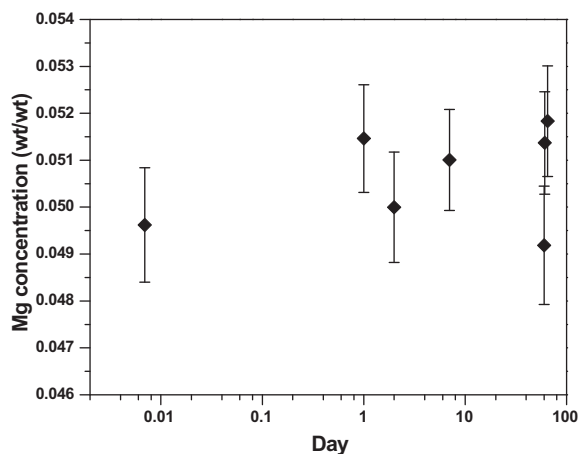
Fig. 4. Concentration of Mg in saturated Mg solution determined by isotope dilution for experimental run that was analogous to Experiments 20A and 20B.

experiments. Correspondingly, the Mg isotope fractionation factors ($\Delta^{26}Mg_{eps-sol}$) increased from $\sim 0‰$ to $\sim 0.6‰$ after 1–7 days and stabilized afterwards. By contrast, the starting

epsomite and $MgSO_4$ solution had distinct $\delta^{25}Mg$ values and these values converged within 1–7 days and then remained constant during additional re-crystallization. For A-series experiments (7A, 20A, and 40A), the ^{25}Mg-enriched starting $MgSO_4$ solutions had an initial $\delta^{25}Mg$ value of 18–19‰ and a Mg molar proportion of 61–70%, relative to that of the initial epsomite ($\delta^{25}Mg = -0.27 \pm 0.10‰$; Mg molar proportion of 30–39%), and these values converged towards 11–12‰. For B-series experiments (7B, 20B, and 40B), the ^{25}Mg-enriched starting epsomite had an initial $\delta^{25}Mg$ value of $18.74 \pm 0.06‰$ and a molar proportion of 30–39% relative to that of the starting $MgSO_4$ solution ($\delta^{25}Mg = -0.2$ to $-0.3‰$; Mg molar proportion of 61–70%), and these values converged towards 5–6‰. Changes in $\delta^{25}Mg$ values were accompanied by changes in the *apparent* measured Mg isotope fractionation factors, where the initial $\Delta^{25}Mg_{eps-sol}$ changed from $\sim -19‰$ (for A-series experiments) or $\sim 19‰$ (for B-series experiments) to $\sim 0.3‰$ at the end of the experiments.

Despite the similarity in the general temporal trends of $\delta^{26}Mg$ and $\delta^{25}Mg$ values in the experiments, there are differences in the time over which $\delta^{26}Mg$ and $\delta^{25}Mg$ values of the epsomite and $MgSO_4$ solution converged to constant values. In general, for a given temperature, it took less time

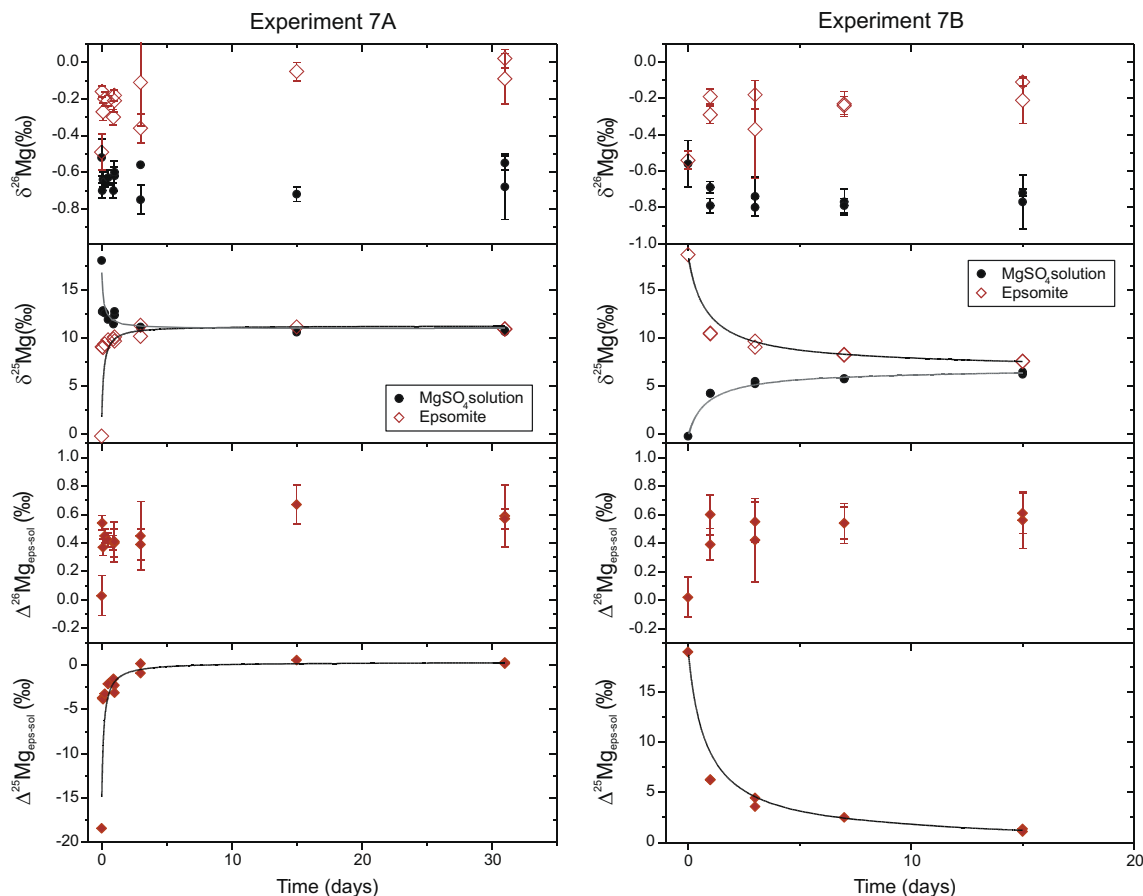Fig. 5. Plots of $\delta^{26}Mg$ and $\delta^{25}Mg$ values of epsomite and $MgSO_4$ solution, as well as $\Delta^{26}Mg_{eps-sol}$ and $\Delta^{25}Mg_{eps-sol}$ fractionations, as a function of time for experiments at 7 °C. The solid lines show the values of $\delta^{25}Mg_{eps}$, $\delta^{25}Mg_{sol}$ and $\Delta^{25}Mg_{eps-sol}$ predicted using the second-order rate constant obtained by regression (for details, see Section 5.1).
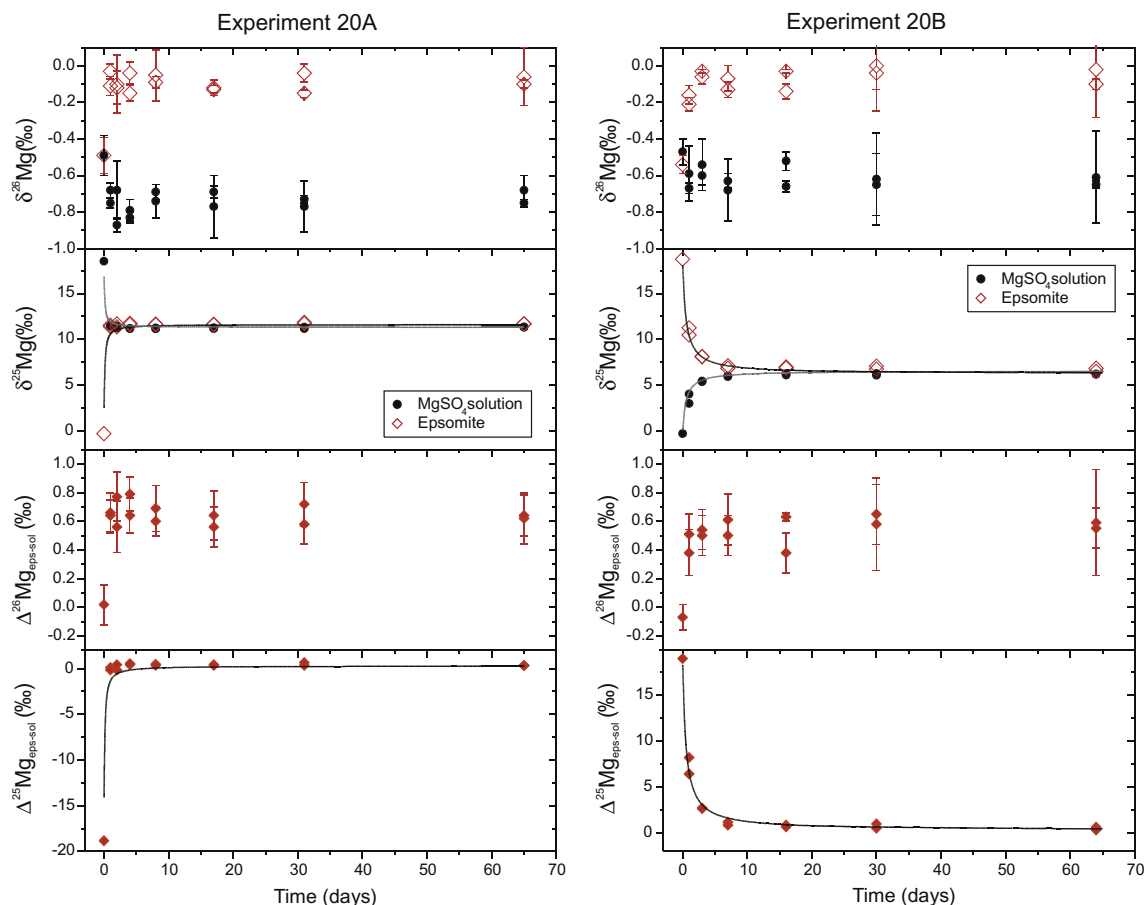
Fig. 6. Plots of δ^{26}Mg and δ^{25}Mg values of epsomite and MgSO$_4$ solution, as well as Δ^{26}Mg$_{eps–sol}$ and Δ^{25}Mg$_{eps–sol}$ fractionations, as a function of time for experiments at 20 °C. The solid lines show the values of δ^{25}Mg$_{eps}$, δ^{25}Mg$_{sol}$ and Δ^{25}Mg$_{eps–sol}$ predicted using the second-order rate constant obtained by regression (for details, see Section 5.1).

for the δ^{26}Mg and δ^{25}Mg values to stabilize in experiment series A. For the same experiment series (either A or B), the experiments at 20 °C reached a stable isotopic composition faster than those at 7 °C. Quantitative discussion of the isotope exchange in these experiments is provided in the next section.

5. DISCUSSION

5.1. Kinetics of Mg isotope exchange

The kinetics of Mg isotope exchange between solution and epsomite were constrained using ^{25}Mg-enriched tracers. Following approaches taken by previous studies (e.g., Johnson et al., 2002; Welch et al., 2003), the degree of isotope exchange toward isotopic equilibrium is defined by:

$$F = (\delta_t - \delta_i)/(\delta_e - \delta_i) \tag{5}$$

where δ_t is the isotopic composition at a given time t, and δ_i and δ_e are the initial and equilibrium isotopic compositions, respectively. In a two-component isotope exchange experiment, F can be calculated from the isotopic compositions of either phase and the two F values are expected to be the same. In this study, calculation of F using δ^{25}Mg data

from epsomite or MgSO$_4$ solution yields consistent results (Electronic Appendix 4). The δ_e value is determined from the isotopic mass-balance of the starting materials and further corrected for mass-dependent isotopic fractionation between epsomite and MgSO$_4$ solution by iteration (Matthews et al., 1983b). In our previous work (e.g., Johnson et al., 2002; Welch et al., 2003) we did not make this correction because the isotopic contrast between the two components was much greater (∼460‰ per mass unit difference) as compared to this study, where the isotopic contrast was only ∼19‰ per mass unit difference.

Substituting F into the general rate equation produces:

$$-d(1 - F)/dt = k_n(1 - F)^n \tag{6}$$

Where k_n is the rate constant and n is the order of the reaction that is generally an integer from 0 to 3. Most isotope exchange reactions have been reported to follow a first-order ($n = 1$) or second-order ($n = 2$) rate law (e.g., Huang and Tsai, 1970; Graham, 1981; Criss et al., 1987; Johnson et al., 2002; Welch et al., 2003). The integrated forms of the first-order and second-order rate functions are:

$$\ln(1 - F) = -k_1 t \quad \text{for } n = 1 \tag{7}$$
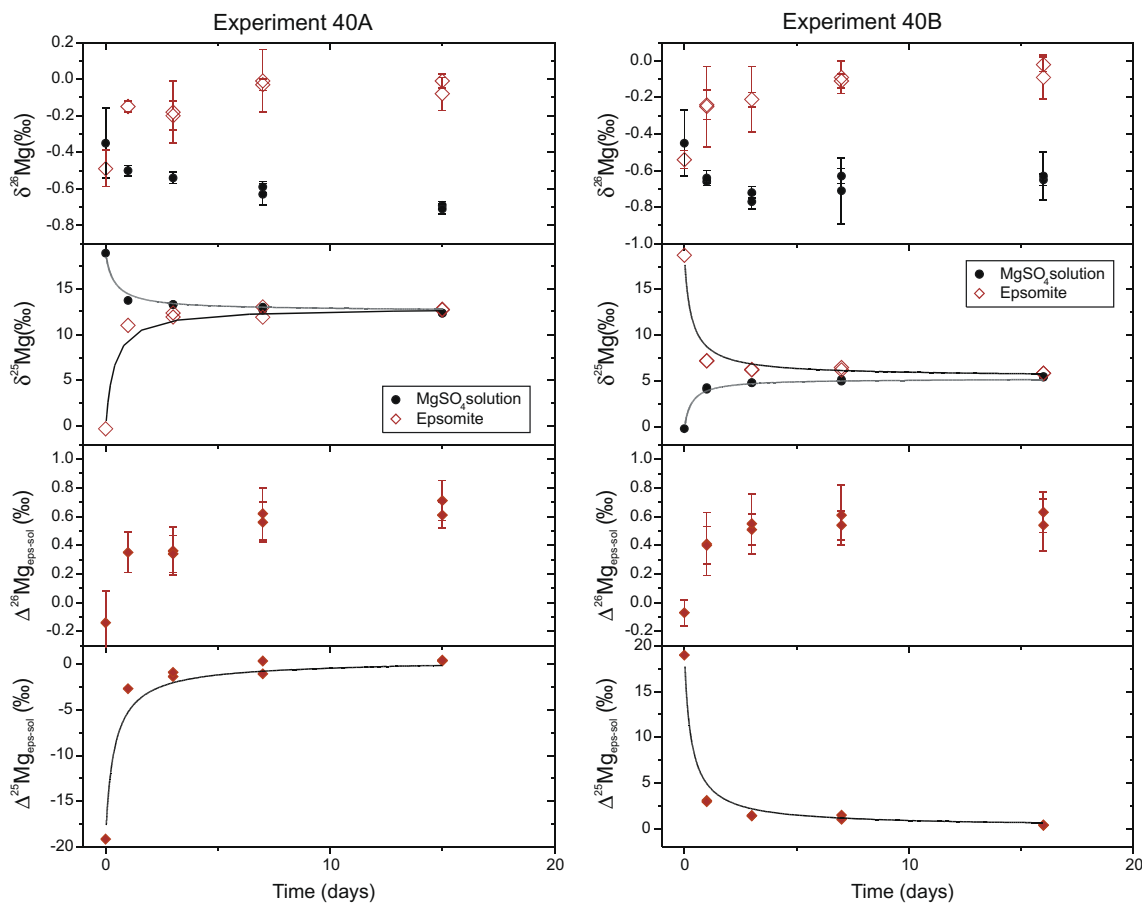
$$F/(1 - F) = k_2 t \quad \text{for } n = 2 \tag{8}$$

Fig. 7. Plots of $\delta^{26}Mg$ and $\delta^{25}Mg$ values of epsomite and $MgSO_4$ solution, as well as $\Delta^{26}Mg_{eps-sol}$ and $\Delta^{25}Mg_{eps-sol}$ fractionations, as a function of time for experiments at 40 °C. The solid lines show the values of $\delta^{25}Mg_{eps}$, $\delta^{25}Mg_{sol}$ and $\Delta^{25}Mg_{eps-sol}$ predicted using the second-order rate constant obtained by regression (for details, see Section 5.1).

The Mg isotope exchange data in this study are better fit by a second-order rate law than a first-order law (Fig. 8). An intercept at $t = 0$ of zero is required for both a 1st and 2nd order rate law, and for Experiment 7B, the R^2 of regressions with a zero intercept are 0.12–0.29 for first-order rate law and 0.77–0.99 for second-order rate law. The rate constants for the different recrystallization experiments were obtained by regression of the best-fitting second-order rate function, and the rate constants are tabulated in Table 3. In each experiment, the reaction constants calculated from F values were used to construct the theoretical values of $\delta^{25}Mg_{eps}$, $\delta^{25}Mg_{sol}$ and $\Delta^{25}Mg_{eps}$ with time. The calculated curves match the measured data points well (Figs. 5–7).

A detailed discussion of the implications of first- or second-order rate laws as applied to the current experiments is beyond the scope of this paper, and instead we use the derived rate constants to address the question of equilibrium or kinetic isotope fractionation upon isotopic exchange. Although the "three-isotope method" is an excellent approach for determining the extent of isotopic exchange, it does not strictly prove attainment of isotopic equilibrium. For example, if 100% exchange occurs via very rapid dissolution and re-precipitation, it is possible that the measured

isotopic fractionation reflects a kinetic isotope effect imposed by limits of ion dehydration and advancing crystallization fronts, which produce isotopic gradients in solution. It is important to stress that 100% isotopic exchange is not the same as attainment of equilibrium, mass-dependent isotopic fractionation if exchange occurred under kinetically controlled conditions, and there is some confusion on these points in the literature. It is certainly possible, for example, that the increase in crystal size that occurs during Ostwald ripening could occur quickly enough so that Mg isotope equilibrium between the crystal surface and the fluid was not maintained. Such a condition could produce isotopic compositions that plot on the secondary fractionation line (Fig. 1), indicating 100% exchange, but $\Delta^{26}Mg_{A-B}$ and $\Delta^{25}Mg_{A-B}$ fractionation factors could reflect, at least in part, kinetic fractionations.

We assess the possibility that complete or near-complete Mg isotope exchange was associated with kinetic, mass-dependent fractionation through comparison of the second-order rate constants and the experiment conditions in terms of grain size of epsomite, temperature, and agitation methods. Under the same temperature and agitation method, experiments that used finer-grained starting epsomite yielded higher rate constants than experiments that
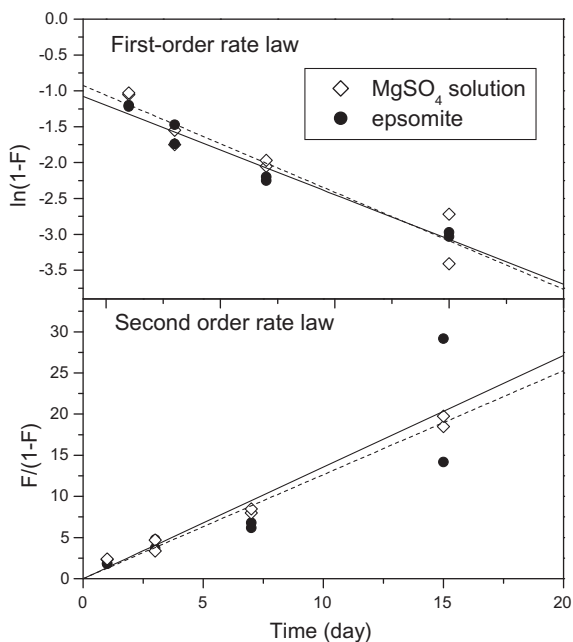
Fig. 8. Plots of the Mg isotope exchange data in Experiment 7B using first-order rate and second-order rate laws. Solid lines are regression lines for Mg isotope data of epsomite, dashed lines are regression lines for Mg isotope data of MgSO₄ solution.

involved coarser-grained epsomite. For example, k_{7a} is about 6–7 times greater than k_{7b}, and k_{20a} is about 4–5 times greater than k_{20b} (Table 3), and this correlates with the smaller initial epsomite crystals of Experiments 7A and 20A (Table 1). Comparison of the same starting epsomite crystal size and agitation method, isotopic exchange was faster at higher temperature (Table 3). Relations between rates of isotope exchange and crystal size and temperature are well documented in the literature (e.g., Matthews et al., 1983b; Zhang, 2008). Finally, the mechanism of agitation can have an influence on the rate constant. Agitation was used in all experiments to minimize generation of static boundary layers or pore volumes. The high temperature (40 °C) experiments required an orbital shaker, whereas

the lower temperature experiments were better suited to use of a horizontal roller. The rate constant for Experiment 40B is higher than the 20B and 7B experiments which would be predicted based on temperature changes. However, for 40A, the rate constant is low relative to that expected for the high temperature conditions (Table 3) and this may be due to compaction that may have preferentially occurred for finer-grained epsomite crystals coupled with the lower suspension efficiency of the orbital shaker compared to the roller. Once compaction occurs, the surface area available for isotope exchange would be significantly limited.

5.2. Mg isotope fractionation factor between epsomite and saturated MgSO₄ solution

The three-isotope method permits determination of the isotope fractionation factor in a two-component system that has undergone partial isotopic exchange through extrapolation to a fractionation factor at 100% exchange (e.g., Matsuhisa et al., 1978; Matthews et al., 1983a,b). Extrapolation is generally illustrated on a three-isotope plot, which in the case of Mg, would be a $^{26}Mg/^{24}Mg$-$^{25}Mg/^{24}Mg$ diagram, through projection of exchange trajectories from initial compositions to a secondary mass-fractionation line (Electronic Appendix 5); numerous examples of this approach exist for O and Fe isotopes (e.g., Matsuhisa et al., 1978; Matthews et al., 1983a,b; Shahar et al., 2008; Beard et al., 2010). Uncertainties, however, are introduced using a traditional three-isotope plot if different time points have changes in molar mass balance between the two components, as may occur, for example, in non-representative sampling of a single large reactor, or if different reactors are used for each time point and there is some variability in initial moles of reactants. In this study, we recast the three-isotope exchange rates in terms of fraction of exchange (F) for the two components, which eliminates variability due to small differences in the Mg molar ratio of epsomite and solution for each reactor. Extrapolation of the $\delta^{26}Mg$ values of epsomite and MgSO₄ solutions to an F value of 100 percent isotope exchange permits a rigorous determination of the Mg isotope fractionation factor and associated uncertainties (Fig. 9 and Table 3).

Table 3
Summary of isotopic exchange-rate constants and Mg isotope fractionation factors of the experiments.

| Experiment ID		Second-order rate law constant (day⁻¹)		Isotope fractionation factor	
		K	1 SE	$\Delta^{26}Mg_{eps–sol}$	2 SD
7A	Solution:	7.18	2.07	0.65	0.04
	Epsomite:	9.88	2.02		
7B	Solution:	1.36	0.18	0.60	0.05
	Epsomite:	1.26	0.04		
20A	Solution:	11.68	1.67	0.52	0.07
	Epsomite:	12.85	3.97		
20B	Solution:	3.10	0.12	0.63	0.07
	Epsomite:	2.38	0.51		
40A	Solution:	3.89	0.11	0.55	0.07
	Epsomite:	2.97	0.68		
40B	Solution:	4.37	0.20	0.57	0.06
	Epsomite:	6.63	1.17		
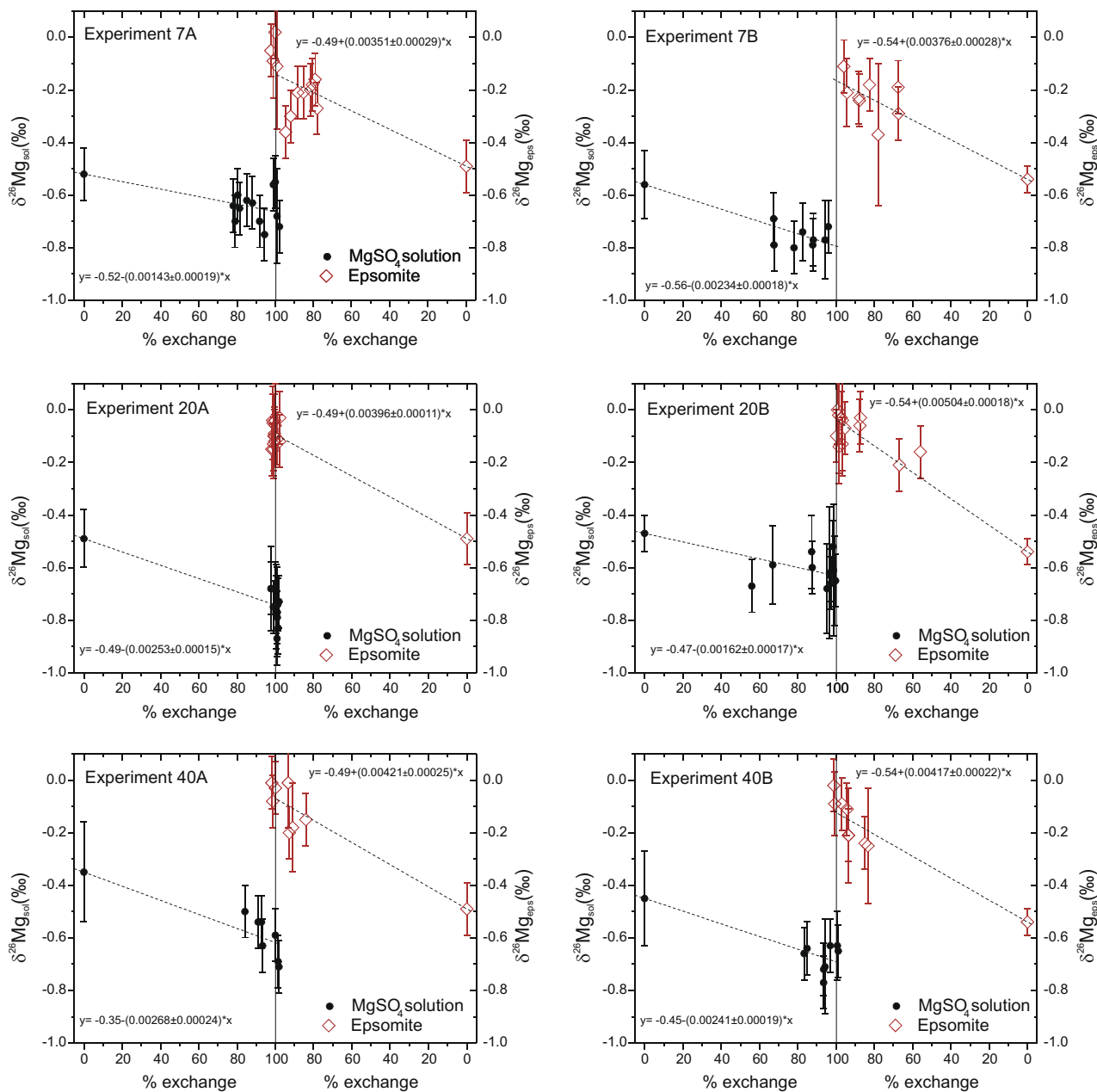
Fig. 9. Plot of $\delta^{26}Mg$ values of epsomite and $MgSO_4$ solutions as a function of degree of isotope exchange in the recrystallization experiments. The extrapolation lines were forced through the points of the starting materials; the regression function was obtained using Origin®.

As shown in Table 3, for experiments at the same temperature, the $\Delta^{26}Mg_{eps-sol}$ values are indistinguishable within error, despite the many-fold difference in the exchange-rate constants. Kinetic effects on oxygen isotope fractionation during carbonate synthesis have been recognized to correlate with precipitation rates (e.g., de Villiers et al., 1995; Kim et al., 2006, 2009; Dietzel et al., 2009), and Ca isotope fractionation factors during calcite precipitation have been interpreted to be related to precipitation rates, reflecting kinetic isotope effects (Lemarchand et al., 2004). The independence of the $\Delta^{26}Mg_{eps-sol}$ fractionations relative to reaction rate implies attainment of isotopic equilibrium in these experiments. We note that it is not possible

to infer kinetic versus equilibrium fractionation based on differences in mass-dependent $^{26}Mg/^{24}Mg$ – $^{25}Mg/^{24}Mg$ fractionation lines (e.g., Young et al., 2002; Young and Galy, 2004) because we used enriched isotope tracers.

The $\Delta^{26}Mg_{eps-sol}$ fractionations at different temperatures are essentially indistinguishable within error (Table 3). Combining the results from A and B-series experiments, the $\Delta^{26}Mg_{eps-sol}$ fractionation is $0.63 \pm 0.07‰$ at 7 °C, $0.58 \pm 0.16‰$ at 20 °C and $0.56 \pm 0.03‰$ at 40 °C. The relative insensitivity of the $\Delta^{26}Mg_{eps-sol}$ fractionation factor to temperature likely reflects the small magnitude of the fractionation factor at low temperatures. Equilibrium isotope fractionations generally decrease as temperature

increases, in proportion to $1/T^2$ for most cases (Bigeleisen and Mayer, 1947; Urey, 1947; O'Neil, 1986; Schauble, 2004). The function of the best-fitting regression line for the data in a $\Delta^{26}Mg$–$1/T^2$ diagram (Fig. 10), assuming zero fractionation at infinite temperature, is:

$$\Delta^{26}Mg_{eps-sol} = 0.0510(\pm0.0026) \times 10^6/T^2 \qquad (9)$$

This function should be valid for extrapolating to different temperatures, assuming a $1/T^2$ relation is valid and that there are no reversals in the epsomite-solution fractionation factor. Note that in practice, T should be confined to the stability region of epsomite (between 1.8 and 48.3 °C under 1 bar pressure). $\Delta^{26}Mg_{eps-sol}$ fractionations calculated using Eq. 9 are calculated to be 0.65‰ at 7 °C, 0.57‰ at 20 °C and 0.52‰ at 40 °C, and these lie within error of those measured in the experiments.

Recently, Schauble (2010) calculated the reduced partition function ratios (RPFR) for $^{26}Mg/^{24}Mg$ for aqueous Mg and a number of minerals including meridianiite ($MgSO_4\cdot11H_2O$) by *ab initio* quantum mechanical calculations, and predicted that the $\Delta^{26}Mg_{mer-sol}$ fractionation is +0.3‰ at 20 °C (Fig. 10). We suggest that there should be little difference in the RPRF for Mg in meridianiite and epsomite because water molecules are weakly attached in both minerals. If the RPFR of $^{26}Mg/^{24}Mg$ for meridianiite ($MgSO_4\cdot11H_2O$) by Schauble (2010) is combined with the RPFR of $^{26}Mg/^{24}Mg$ for aqueous Mg calculated separately by Rustad et al. (2010), the predicted $\Delta^{26}Mg_{mer-sol}$

Fig. 10. Plot of Mg isotope fractionation factor between Mg-sulfates and MgSO₄ solution ($\Delta^{26}Mg_{min-sol}$) as a function of $10^6/T^2$ (T in K). The solid line denotes the best-fitting regression line for the data of experiments for epsomite, where the line is forced through the origin, and the thin dashed lines denote the upper and lower 95% confidence limits of the regression. The solid grey line denotes the predicted Mg isotope fractionation between meridianiite ($MgSO_4\cdot11H_2O$) and MgSO₄ solution using the reduced partition function ratios (RPFR) of $^{26}Mg/^{24}Mg$ for meridianiite and aqueous Mg by calculated by Schauble (2010). The dashed grey line denotes the predicted Mg isotope fractionation between meridianiite ($MgSO_4\cdot11H_2O$) and MgSO₄ solution using the RPFR of $^{26}Mg/^{24}Mg$ for meridianiite calculated by Schauble (2010) and RPFR of $^{26}Mg/^{24}Mg$ for aqueous Mg by Rustad et al. (2010).

fractionation is +2.2‰ at 20 °C (Fig. 10). Although the discrepancy between the two predictions for meridianiite–aqueous fractionation factors indicates discrepancies in predicted RPFRs for aqueous Mg that must be resolved, the positive direction of predicted Mg isotope fractionations in meridianiite is consistent with epsomite determined in this study. Compared to heavier metal sulfates, Li et al. (2008) measured the Cu isotope fractionation factor between chalcanthite ($CuSO_4\cdot5H_2O$) and saturated $CuSO_4$ solution, which they determined to produce a $\Delta^{65}Cu_{cha-sol}$ fractionation of 0.17‰. This, in addition the present study, suggests that heavier isotopes of metal ions preferentially partition into sulfates relative to aqueous species. The smaller Cu isotope fractionation relative to that of Mg generally follows that expected relative to mass (e.g., O'Neil, 1986; Schauble, 2004).

The current study indicates that Mg isotopes in sulfates fractionate in the opposite direction between Mg-bearing calcite and aqueous solution. A number of field and laboratory studies have shown that Mg in inorganically precipitated calcite is isotopically lighter than Mg in aqueous solution by 2–3‰ in $\delta^{26}Mg$ (e.g., Galy et al., 2002; Kisakurek et al., 2009; Immenhauser et al., 2010). The Mg isotope fractionation measured in this study provides some qualitative insight into the bonding of the metal cation in mineral-aqueous systems. In both carbonate-solution and epsomite-solution systems, Mg^{2+} in aqueous solutions are hydrated, where each Mg^{2+} is bonded to six H_2O molecules to form an octahedral aquo ion ($[Mg(OH_2)_6]^{2+}$) (Richens, 1997). The $[Mg(OH_2)_6]^{2+}$ octahedron is retained in the epsomite structure, and bonds SO_4^{2-} and a "spare" seventh H_2O molecule with hydrogen bonds to form a stable mineral (Fortes, 2005). In contrast, there is no H_2O molecule in the carbonate lattice, and Mg^{2+} must dehydrate before bonding with CO_3^{2-} to form carbonate. We speculate that the positive values for $\Delta^{26}Mg_{eps-sol}$ may reflect stronger hydrogen bonds on $[Mg(OH_2)_6]^{2+}$ octahedra in epsomite than in MgSO₄ solution. The negative values for $\Delta^{26}Mg_{carb-sol}$ may reflect the difference in strength and configuration of bonds directly on Mg^{2+} ions between aqueous solution and carbonates (Rustad et al., 2010; Schauble, 2010), and/or kinetic isotope effects during dehydration of $[Mg(OH_2)_6]^{2+}$ aquo ions in carbonate precipitation (Immenhauser et al., 2010).

5.3. Applications
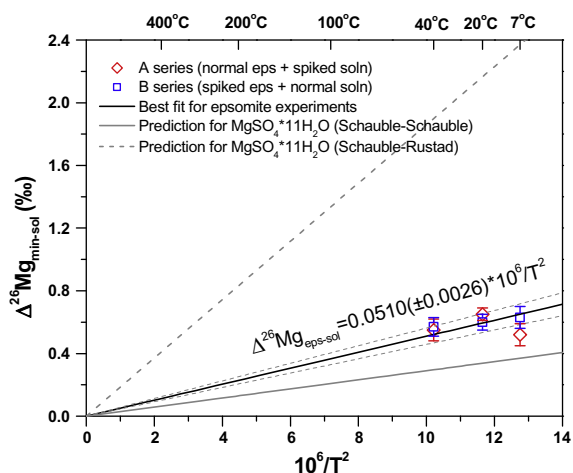
The relatively small epsomite–solution Mg isotope fractionation factor, coupled with the modest influence of evaporite formation on the Mg budget in Earth's ocean (Holland, 1984; Wolery and Sleep, 1988; Wilkinson and Algeo, 1989; Berner and Berner, 1996), indicates that the Earth's oceanic Mg isotope composition is not likely to be influenced by evaporite formation. Instead, the results here suggest that Mg isotopes may be a sensitive indicator of the extent of evaporite precipitation in a confined system such as a salt lake or lagoon. To illustrate the use of Mg isotopes to trace evaporite evolution, a simple model is constructed, where it is assumed that (1) the Mg isotope composition of the starting reservoir and possible Mg influx

equals that of seawater (δ^{26}Mg = −0.8‰, Tipper et al., 2006, 2008; Hippler et al., 2009), and (2) epsomite is the dominant Mg-bearing evaporite and Δ^{26}Mg$_{eps–sol}$ is 0.6‰. In a closed system, the Mg isotope composition of evaporite follows a Rayleigh fractionation behavior, and the δ^{26}Mg values of epsomite reaches as low as −2‰ when 95% of the Mg is precipitated (Fig. 11). By contrast, when the system is partly open to an influx of replenished Mg, such as may occur in an inland salt lake or a lagoon, the decrease in δ^{26}Mg values of epsomite relative to the degree of evaporation is much less dramatic (Fig. 11). For example, in a system where the influx of Mg is 70% of the Mg loss by evaporation, the δ^{26}Mg value of epsomite is about −1‰ when 95% of the Mg is precipitated. In a restricted basin setting, these models show that it is difficult to reconstruct the Mg isotope composition of seawater from evaporites. Because, however, the δ^{26}Mg values of epsomite decreases monotonically in all cases, the Mg isotope composition of evaporite can be used as an effective means for distinguishing drought-wet cycles of an evaporative ancient basin, where the lowest δ^{26}Mg values would represent the cessation of an evaporation event at the end of a drought, whereas an increase in δ^{26}Mg values in subsequent evaporites would record a wetter period and an influx of Mg-bearing fluids.

It should be noted that carbonate is an important component of the mineral assemblage of precipitates during evaporation of seawater and development of brines on Earth, because Mg also partitions into carbonates and significant Mg isotope fractionations have been reported between carbonates and solution (Galy et al., 2002; Chang et al., 2004; Pogge von Strandmann, 2008; Hippler et al., 2009). Precipitation of carbonates, therefore, may add to the complexity of the Mg isotope systematics in evaporites, but this can be evaluated based on the lithologies present in an evaporite sequence. In contrast, carbonates may have been less important in the evaporite sequences on Mars, because evidence so far suggests that the sulfur cycle, instead of a carbon cycle, dominated surficial processes on ancient Mars (McLennan et al., 2007; Wang et al., 2009). The significance of Mg sulfates on the Martian surface (e.g., Wang et al., 2008) suggests that the Mg isotope compositions of evaporites from Mars would provide important constraints on the evaporative history of early Mars.

6. CONCLUSIONS

Magnesium isotope fractionation between epsomite and aqueous MgSO$_4$ solution has been constrained by a set of three-isotope experiments, which demonstrate that complete or near-complete Mg isotope exchange was achieved within 14 days in all experiments. Isotopic exchange was driven by recrystallization of epsomite, during which the net Mg transfer was insignificant compared with the mass of Mg that underwent isotopic exchange. The Mg isotope exchange rate between epsomite and MgSO$_4$ solution is dependent on the temperature, grain size of initial epsomite, and agitation methods used in the experiments. As expected, isotopic exchange rates were greatest at high temperature, and when a smaller grain size was used for the initial epsomite. The measured epsomite-solution Mg isotope fractionation factors are inferred to reflect equilibrium conditions because they were independent of the rate of recrystallization. Equilibrium Mg isotope fractionation factors between epsomite and aqueous MgSO$_4$ solution at experiments at 7, 20, and 40 °C were indistinguishable within error, as the Δ^{26}Mg$_{eps–sol}$ fractionations cluster around 0.6‰.

APPENDIX A. SUPPLEMENTARY DATA

Supplementary data associated with this article can be found, in the online version, at doi:10.1016/j.gca.2011.01.023.
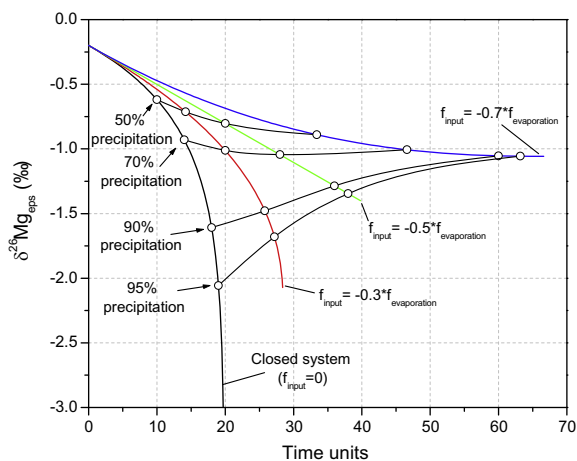

Fig. 11. Modeling results showing the influence of epsomite precipitation and external Mg input on the Mg isotope composition of the evaporite. The δ^{26}Mg value of the starting solution and Mg input are both set as −0.8‰, a modern seawater value, and the Mg isotope fractionation factor (Δ^{26}Mg$_{eps–sol}$) is set as 0.6‰, based on the results of this study. Evaporation is set at a constant rate in all the models, such that in a closed system, all the MgSO$_4$ precipitates after 20 time units.

REFERENCES

Albarède F. and Beard B. (2004) Analytical methods for non-traditional isotopes. In *Geochemistry of Non-Traditional Stable Isotopes*, vol. 55, Mineralogical Soc America. pp. 113–152.

Archer D. G. and Rard J. A. (1998) Isopiestic investigation of the osmotic and activity coefficients of aqueous MgSO$_4$ and the solubility of MgSO$_4$*7H$_2$O(cr) at 298.15 K: thermodynamic properties of the MgSO$_4$ + H$_2$O system to 440 K. *J. Chem. Eng. Data* **43**(5), 791–806.

Beard B. L., Handler R. M., Scherer M. M., Wu L., Czaja A. D., Heimann A. and Johnson C. M. (2010) Iron isotope fractionation between aqueous ferrous iron and goethite. *Earth Planet. Sci. Lett.* **295**(1–2), 241–250.

Berner E. K. and Berner R. A. (1996) *Global Environment: Water, Air, and Geochemical Cycles*. Prentice Hall.

Bigeleisen J. and Mayer M. G. (1947) Calculation of equilibrium constants for isotopic exchange reactions. *J. Chem. Phys.* **15**(5), 261–267.

Bolou-Bi E. B., Poszwa A., Leyval C. and Vigier N. (2010) Experimental determination of magnesium isotope fractionation during higher plant growth. *Geochim. Cosmochim. Acta* **74**(9), 2523–2537.

Chang V. T. C., Williams R. J. P., Makishima A., Belshawl N. S. and O'Nions R. K. (2004) Mg and Ca isotope fractionation during CaCO$_3$ biomineralisation. *Biochem. Biophys. Res. Commun.* **323**(1), 79–85.

Chauhan U. P. S. and Ray Sarkar B. C. (1969) Use of calmagite for the determination of traces of magnesium in biological materials. *Anal. Biochem.* **32**(1), 70–80.

Chou I. M. and Seal R. R. (2003) Determination of epsomite–hexahydrite equilibria by the humidity-buffer technique at 0.1 MPa with implications for phase equilibria in the system MgSO$_4$–H$_2$O. *Astrobiology* **3**(3), 619–630.

Clark B. C., Morris R. V., McLennan S. M., Gellert R., Jolliff B., Knoll A. H., Squyres S. W., Lowenstein T. K., Ming D. W., Tosca N. J., Yen A., Christensen P. R., Gorevan S., Bruckner J., Calvin W., Dreibus G., Farrand W., Klingelhoefer G., Waenke H., Zipfel J., Bell Iii J. F., Grotzinger J., McSween H. Y. and Rieder R. (2005) Chemistry and mineralogy of outcrops at Meridiani Planum. *Earth Planet. Sci. Lett.* **240**(1), 73–94.

Criss R. E., Gregory R. T. and Taylor, Jr., H. P. (1987) Kinetic theory of oxygen isotopic exchange between minerals and water. *Geochim. Cosmochim. Acta* **51**(5), 1099–1108.

de Villiers S., Nelson B. K. and Chivas A. R. (1995) Biological controls on coral Sr/Ca and δ^{18}O reconstructions of sea surface temperatures. *Science* **269**(5228), 1247–1249.

Dietzel M., Tang J., Leis A. and Kohler S. J. (2009) Oxygen isotopic fractionation during inorganic calcite precipitation – effects of temperature, precipitation rate and pH. *Chem. Geol.* **268**(1–2), 107–115.

Fortes A. D. (2005) From surrey to the moons of Jupiter (via Mars): the story of epsomite. *Axis* **1**(9), 1–28.

Galy A., Bar-Matthews M., Halicz L. and O'Nions R. K. (2002) Mg isotopic composition of carbonate: insight from speleothem formation. *Earth Planet. Sci. Lett.* **201**(1), 105–115.

Galy A., Yoffe O., Janney P. E., Williams R. W., Cloquet C., Alard O., Halicz L., Wadhwa M., Hutcheon I. D., Ramon E. and Carignan J. (2003) Magnesium isotope heterogeneity of the isotopic standard SRM980 and new reference materials for magnesium-isotope-ratio measurements. *J. Anal. At. Spectrom.* **18**(11), 1352–1356.

Graham C. M. (1981) Experimental hydrogen isotope studies. III: Diffusion of hydrogen in hydrous minerals, and stable isotope exchange in metamorphic rocks. *Contrib. Mineral. Petrol.* **76**(2), 216–228.

Hardie L. A. (1990) The roles of rifting and hydrothermal CaCl$_2$ brines in the origin of potash evaporites: an hypothesis. *Am. J. Sci.* **290**, 43–106.

Higgins J. A. and Schrag D. P. (2010) Constraining magnesium cycling in marine sediments using magnesium isotopes. *Geochim. Cosmochim. Acta* **74**(17), 5039–5053.

Hippler D., Buhl D., Witbaard R., Richter D. K. and Immenhauser A. (2009) Towards a better understanding of magnesium-isotope ratios from marine skeletal carbonates. *Geochim. Cosmochim. Acta* **73**(20), 6134–6146.

Holland H. D. (1984) *The Chemical Evolution of the Atmosphere and Oceans*. Princeton University Press.

Huang F., Glessner J., Ianno A., Lundstrom C. and Zhang Z. (2009) Magnesium isotopic composition of igneous rock standards measured by MC-ICP-MS. *Chem. Geol.* **268**(1–2), 15–23.

Huang T.-C. and Tsai F.-N. (1970) Kinetic studies on the isotopic exchange of calcium ion and calcium carbonate. *J. Inorg. Nucl. Chem.* **32**(1), 17–31.

Immenhauser A., Buhl D., Richter D., Niedermayr A., Riechelmann D., Dietzel M. and Schulte U. (2010) Magnesium-isotope fractionation during low-Mg calcite precipitation in a limestone cave – field study and experiments. *Geochim. Cosmochim. Acta* **74**(15), 4346–4364.

Johnson C. M., Skulan J. L., Beard B. L., Sun H., Nealson K. H. and Braterman P. S. (2002) Isotopic fractionation between Fe(III) and Fe(II) in aqueous solutions. *Earth Planet. Sci. Lett.* **195**(1–2), 141–153.

Kim S.-T., Hillaire-Marcel C. and Mucci A. (2006) Mechanisms of equilibrium and kinetic oxygen isotope effects in synthetic aragonite at 25 °C. *Geochim. Cosmochim. Acta* **70**(23), 5790–5801.

Kim S.-T., Kang J. O., Yun S.-T., O'Neil J. R. and Mucci A. (2009) Experimental studies of oxygen isotope fractionation between rhodochrosite (MnCO$_3$) and water at low temperatures. *Geochim. Cosmochim. Acta* **73**, 4400–4408.

Kisakurek B., Niedermayr A., Moeller M. N., Taubner I., Eisenhauer A., Dietzel M., Buhl D., Fietzke J. and Erez J. (2009) Magnesium isotope fractionation in inorganic and biogenic calcite. *Geochim. Cosmochim. Acta* **73**, A663.

Lemarchand D., Wasserburg G. J. and Papanastassiou D. A. (2004) Rate-controlled calcium isotope fractionation in synthetic calcite. *Geochim. Cosmochim. Acta* **68**(22), 4665–4678.

Li J., Zhu X. K. and Tang S. H. (2008) Experimental study on Cu isotope fractionation during crystallization and reduction at low temperatures. *Geochim. Cosmochim. Acta* **72**(12), A540.

Li W.-Y., Teng F.-Z., Ke S., Rudnick R. L., Gao S., Wu F.-Y. and Chappell B. W. (2010) Heterogeneous magnesium isotopic composition of the upper continental crust. *Geochim. Cosmochim. Acta* **74**, 6867–6884.

Matsuhisa Y., Goldsmith J. R. and Clayton R. N. (1978) Mechanisms of hydrothermal crystallization of quartz at 250 °C and 15 kbar. *Geochim. Cosmochim. Acta* **42**(2), 173–182.

Matthews A., Goldsmith J. R. and Clayton R. N. (1983a) On the mechanisms and kinetics of oxygen isotope exchange in quartz and feldspars at elevated temperatures and pressures. *Geol. Soc. Am. Bull.* **94**(3), 396–412.

Matthews A., Goldsmith J. R. and Clayton R. N. (1983b) Oxygen isotope fractionations involving pyroxenes: the calibration of mineral-pair geothermometers. *Geochim. Cosmochim. Acta* **47**(3), 631–644.

McLennan S. M., Arvidson R. E., Clark B. C., Golombek M. P., Grotzinger J. P., Jolliff B. L., Knoll A. H., Squyres S. W., and Tosca N. J. (2007) Geochemistry, mineralogy and diagenesis of the burns formation at Meridiani Planum: Insights into the sedimentary rock cycle on Mars. *Seventh International Conference on Mars*. #3231 (abstr.).

Mullin J. W. (2001) *Crystallization*. Butterworth–Heinemann.

O'Neil J. R. (1986) Theoretical and experimental aspects of isotopic fractionation. *Rev. Mineral.* **16**, 1–40.

Pearson N. J., Griffin W. L., Alard O. and O'Reilly S. Y. (2006) The isotopic composition of magnesium in mantle olivine: records of depletion and metasomatism. *Chem. Geol.* **226**(3–4), 115–133.

Pogge von Strandmann P. A. E. (2008) Precise magnesium isotope measurements in core top planktic and benthic foraminifera. *Geochem. Geophys. Geosyst.* **9**.

Posern K. and Kaps C. (2008) Humidity controlled calorimetric investigation of the hydration of $MgSO_4$ hydrates. *J. Therm. Anal. Calorim.* **92**(3), 905–909.

Richens D. T. (1997) *The Chemistry of Aqua Ions*. John Wiley & Sons.

Rustad J. R., Casey W. H., Yin Q.-Z., Bylaska E. J., Felmy A. R., Bogatko S. A., Jackson V. E. and Dixon D. A. (2010) Isotopic fractionation of Mg^{2+}(aq), Ca^{2+}(aq), and Fe^{2+}(aq) with carbonate minerals. *Geochim. Cosmochim. Acta* **74**(22), 6301–6323.

Schauble E. A. (2004) Applying stable isotope fractionation theory to new systems. In *Geochemistry of Non-Traditional Stable Isotopes*, vol. 55, Mineralogical Soc America, pp. 65–111.

Schauble E. A. (2010) First-principles estimates of equilibrium magnesium isotope fractionation in silicate, oxide, carbonate and hexaaquamagnesium(2+) crystals. *Geochimica et Cosmochimica Acta* **75**, 844–869.

Shahar A., Young E. D. and Manning C. E. (2008) Equilibrium high-temperature Fe isotope fractionation between fayalite and magnetite: an experimental calibration. *Earth Planet. Sci. Lett.* **268**(3–4), 330–338.

Shen B., Jacobsen B., Lee C.-T. A., Yin Q.-Z. and Morton D. M. (2009) The Mg isotopic systematics of granitoids in continental arcs and implications for the role of chemical weathering in crust formation. *Proc. Natl. Acad. Sci. USA* **106**(49), 20652–20657.

Stoffregen R. E., Rye R. O. and Wasserman M. D. (1994) Experimental studies of alunite: II. Rates of alunite–water alkali and isotope exchange. *Geochim. Cosmochim. Acta* **58**(2), 917–929.

Tipper E. T., Galy A., Gaillardet J., Bickle M. J., Elderfield H. and Carder E. A. (2006) The magnesium isotope budget of the modern ocean: constraints from riverine magnesium isotope ratios. *Earth Planet. Sci. Lett.* **250**(1–2), 241–253.

Tipper E. T., Louvat P., Capmas F., Galy A. and Gaillardet J. (2008) Accuracy of stable Mg and Ca isotope data obtained by MC-ICP-MS using the standard addition method. *Chem. Geol.* **257**(1–2), 65–75.

Urey H. C. (1947) The thermodynamic properties of isotopic substances. *J. Chem. Soc.*, 562–581.

Wang A., Bell J. F., III Li R., Johnson J. R., Farrand W. H., Cloutis E. A., Arvidson R. E., Crumpler L., Squyres S. W., McLennan S. M., Herkenhoff K. E., Ruff S. W., Knudson A. T., Chen W. and Greenberger R. (2008) Light-toned salty soils and coexisting Si-rich species discovered by the Mars Exploration Rover Spirit in Columbia Hills. *J. Geophys. Res.* **113**.

Wang A., Freeman J. J. and Jolliff B. L. (2009) Phase transition pathways of the hydrates of magnesium sulfate in the temperature range 50 °C to 5 °C: Implication for sulfates on Mars. *J. Geophys. Res.* **114**.

Welch S. A., Beard B. L., Johnson C. M. and Braterman P. S. (2003) Kinetic and equilibrium Fe isotope fractionation between aqueous Fe(II) and Fe(III). *Geochim. Cosmochim. Acta* **67**(22), 4231–4250.

Wilkinson B. H. and Algeo T. J. (1989) Sedimentary carbonate record of calcium–magnesium cycling. *Am. J. Sci.* **289**(10), 1158–1194.

Wolery T. J. and Sleep N. H. (1988) Interactions of geochemical cycles with the mantle. In *Chemical Cycles in the Evolution of the Earth* (eds. C. B. Gregor, R. M. Garrels, F. T. Mackenzie and J. B. Maynard). Wiley & Sons, pp. 77–103.

Young E. D. and Galy A. (2004) The isotope geochemistry and cosmochemistry of magnesium. *Rev. Mineral. Geochem.* **55**(1), 197–230.

Young E. D., Galy A. and Nagahara H. (2002) Kinetic and equilibrium mass-dependent isotope fractionation laws in nature and their geochemical and cosmochemical significance. *Geochim. Cosmochim. Acta* **66**(6), 1095–1104.

Zhang Y. (2008) *Geochemical Kinetics*. Princeton University Press.

Associate editor: Mark Rehkamper